

**Effects of metal impregnation on ZSM-5 for catalytic upgrading of biofuel intermediates**

Marissa Leshnov

Office of Science, Science Undergraduate Laboratory Internship Program

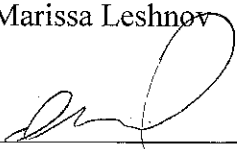
The University of Alabama, Tuscaloosa, AL

National Renewable Energy Laboratory  
Golden, Colorado

May 15, 2015

Prepared in partial fulfillment of the requirement of the Department of Energy, Office of Science's Science Undergraduate Laboratory Internship Program under the direction of Dr. Matthew Yung at the National Renewable Energy Laboratory.

Participant:   
Marissa Leshnov

Research Advisor:   
Matthew Yung

## ABSTRACT

The creation of biofuels via pyrolysis results in an unstable, low quality product, which must be deoxygenated for use as a transportation fuel. Metal impregnation has been studied as a method to develop improved catalysts for use in catalytic upgrading of biofuel intermediates. To investigate the effectiveness of metal impregnation, metal-modified catalysts were prepared via incipient wetness impregnation using Ni, Cu, Pt, Co, and Ga precursors on the zeolite ZSM-5. The physicochemical properties of each catalyst were characterized using ammonia temperature-programmed desorption (NH<sub>3</sub>-TPD), X-ray diffraction (XRD), and Brunauer–Emmett–Teller (BET) surface area analysis, and compared to those of ZSM-5 before use in catalytic upgrading. After performing vapor phase upgrading (VPU) with pine biomass and liquid hydrodeoxygenation (HDO) with anisole as a model compound, catalytic activity was evaluated and coke formation was calculated using thermogravimetric analysis (TGA). Metal-modified catalysts outperformed ZSM-5 during catalytic upgrading by better resisting coke formation and converting a higher percentage of biofuel intermediates. These results suggest that the physical and chemical properties of metal-modified ZSM-5 are ideal for use in catalytic upgrading, thereby advancing the development of superior biofuels.

## I. INTRODUCTION

Biofuels are a cost-effective and sustainable alternative to fossil fuels.<sup>1</sup> One method used to create biofuels is pyrolysis, during which biomass is heated in the absence of oxygen to produce pyrolysis vapors that are then condensed to form raw bio-oil. Bio-oil is not suitable for use as a transportation fuel due to its high oxygen content and low hydrogen-to-carbon ratio, which compromise the quality and stability of the final biofuel product.<sup>2</sup> In order to meet the U.S. Department of Energy's requirements for improved processing of biofuels, biofuel intermediates must have oxygen removed (reducing their acidity) and hydrogen added (improving their energy content). This can be accomplished via catalytic upgrading. During this process, biofuel intermediates are treated with an acidic catalyst in one of two ways: 1) vapor phase upgrading (VPU) of pyrolysis vapors; or 2) hydrodeoxygenation (HDO) of raw bio-oil.<sup>3</sup>

A primary concern during catalytic upgrading is deactivation, which occurs when carbon deposits, or coke, block acid sites on the surface of the catalyst. Researchers agree that coke formation is highly dependent on the conditions of the reaction and the physicochemical features of the catalyst, such as its pore structure and acidity.<sup>3,4</sup> Studies have examined the effects of modifying catalysts by adding metals, termed metal impregnation, as this technique has been found to reduce coke formation on the catalyst while maintaining its product selectivity toward high-energy compounds.<sup>5,6</sup> However, these studies focus only on catalytic upgrading via VPU or HDO, not both. Therefore, it is unclear which metal-modified catalyst is ideal for use in either method of catalytic upgrading.

This study investigated the physical and chemical effects of metal impregnation on a catalyst known as ZSM-5, which belongs to a class of silica-alumina catalysts called zeolites. Zeolites are ideal for use in catalytic upgrading due to their defined pore structure, high acidity, and product selectivity toward aromatics.<sup>4</sup> After characterizing the pore structure, acidity, and

crystalline properties of each catalyst, VPU with biomass and HDO with anisole as a model compound were performed separately in constant reaction conditions to observe catalytic performance and coke formation. It was found that the metal-modified catalysts outperformed ZSM-5 in terms of resisting coke formation and converting biofuel intermediates, suggesting that the physical and chemical properties of these catalysts are ideal for use in catalytic upgrading.

## II. MATERIALS AND METHODS

### A. Catalyst Synthesis

ZSM-5 with a SiO<sub>2</sub>/Al<sub>2</sub>O<sub>3</sub> ratio (SAR) of 30 was obtained from Nexceris for use as a framework and zeolite support. Ni, Cu, Pt, Co, and Ga were added via incipient wetness impregnation. Metal nitrate hydrates were used as precursors for all metals except Pt, which required H<sub>2</sub>PtCl<sub>6</sub>·6H<sub>2</sub>O as a precursor. Metals were introduced to the support at constant molar ratio of 1:2 metal-to-aluminum. After impregnation, the catalysts were dried in an oven at 110 °C and then calcined in air at 550 °C for 3 h.

### B. Catalyst Characterization

The physical and chemical properties of each catalyst were characterized using ammonia temperature-programmed desorption (NH<sub>3</sub>-TPD), X-ray diffraction (XRD), and nitrogen-chemisorption. These techniques were used to evaluate acidity; crystalline structure; and external surface area and pore volume, respectively. The formation of coke on spent catalysts generated from VPU was determined using thermogravimetric analysis (TGA).

#### 1. Ammonia Temperature-Programmed Desorption

NH<sub>3</sub>-TPD was conducted using 100 mg samples in an Altamira AMI-390 system. Ammonia was selected due to its simplicity, small molecular size, and ability to titrate both strong and weak acid sites on the catalyst.<sup>7</sup> Prior to measurements, fresh samples were reduced in a 10% H<sub>2</sub>/Ar stream at 500 °C; spent samples were activated in He at 500 °C for 5 min with a ramp rate of 20 °C/min. All samples were then cooled to 120 °C and saturated in NH<sub>3</sub> by adding 10 volume percent to the He carrier gas for 30 min. After flowing He for 10 min to remove any physically adsorbed NH<sub>3</sub>, TPD was carried out at 500 °C with a ramp rate of 30 °C. A thermal conductivity detector (TCD) determined the concentration of desorbed NH<sub>3</sub>. The samples were then regenerated in O<sub>2</sub> at 600 °C for 30 min with a ramp rate of 20 °C/min before undergoing a second TPD. Upon completion of the experiment, NH<sub>3</sub> was pulsed seven times for calibration.

#### 2. X-ray Diffraction

XRD patterns were obtained with ~20 mg samples at room temperature using a Rigaku Ultima IV device. Cu K<sub>α</sub> radiation was maintained at 40 kV and 44 mA and occurred in the range of 2θ = 5-80° in increments of 0.01°. Average crystalline size was then calculated using the Scherrer equation:

$$\tau = \frac{K\lambda}{\beta \cos\theta} \quad [\text{Eqn. 1}]$$

where the constant  $K$  represents the shape factor (0.9 assuming spherical nanoparticles),  $\lambda$  is X-ray wavelength (1.54 Å for Cu  $K_\alpha$  radiation),  $\beta$  is the full width at half maximum (FWHM) of each diffraction peak in degrees; and  $\theta$  is the peak location given by its diffraction angle.

### 3. Nitrogen-Chemisorption

The adsorption and desorption of nitrogen on each catalyst was measured using a Quadrasorb SI from Quantachrome Instruments. Samples were outgassed under a vacuum at 350 °C overnight and then brought to 77 K via immersion in a liquid nitrogen bath. Total surface area was calculated using multi-point Brunauer–Emmett–Teller (BET) analysis. Pore surface area and pore volume were calculated using Barrett–Joyner–Halenda (BJH) analysis. The t-plot method was used with the DeBoer model for the calculation of the statistical thickness to distinguish the contribution of micropores to the total surface area.

### 4. Thermogravimetric Analysis

TGA of each spent catalyst was completed using a Setsys Evolution TGA-DSC instrument from Setaram. Twenty-milligram samples were stabilized in zero air flowing at 50 mL/min in room temperature for 7 min before heating to 780 °C at 20 °C/min. This temperature was maintained for 20 min before the samples were cooled.

## C. Reaction Procedures

### 1. Catalytic Upgrading via VPU of pine

VPU was conducted in a packed-bed, horizontal quartz reactor in which 500 mg of catalyst was held in place between quartz wool plugs. Upstream of catalyst bed, quartz boats containing 35 mg of pine biomass were inserted into the hot gas stream of 33%  $H_2$  in inert and allowed to pyrolyze. A biomass-to-catalyst ratio of 1:1 was fed over the catalyst by 14 individual pulses of biomass, each separated by ~2.5 min. The pyrolysis vapors were mixed with the reactive flow, swept over the catalyst, and then diluted in a carrier flow of inert gas prior to analysis by the molecular beam mass spectrometer (MBMS), which scanned ions in the mass-to-charge range of  $m/z = 10$ -300. The temperatures of the biomass pyrolysis zone and catalyst upgrading zone were both 500 °C during these experiments, after Shaolong Wan et al.<sup>3</sup> reported that this temperature produces the highest aromatic hydrocarbon yield. A diagram of the reaction system is shown in Figure 1.

Analysis of each pulse of biomass was conducted by averaging 100 MBMS scans, which encompassed the entire pulse of biomass pyrolysis vapors, beginning where the pulse was first observed as indicated by the total ion count. The resulting chromatographs were normalized by the argon signal ( $m/z = 40$ ) in order to minimize any day-to-day variations in system alignment or instrument response.

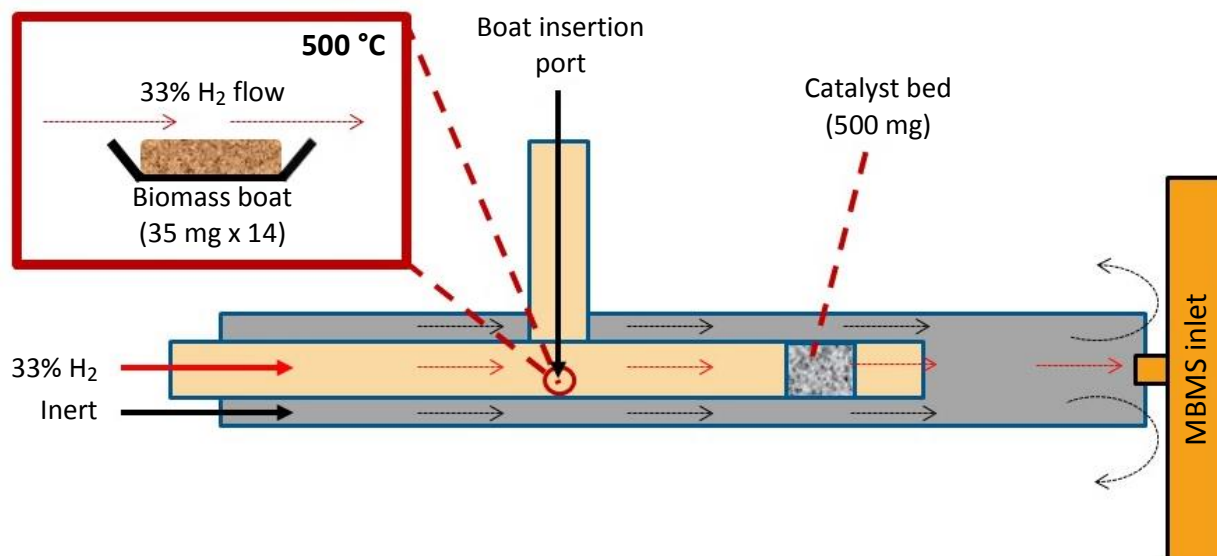


FIG. 1. Schematic of VPU reactor set-up.

## 2. Catalytic Upgrading via HDO of anisole

HDO reaction tests with anisole (Sigma-Aldrich) were carried out in a fixed-bed, vertical reactor in which 100 mg of catalyst was held in place between quartz wool plugs. Prior to experiments, catalysts were reduced in a flow of 75% H<sub>2</sub> in inert gas as the reactor bed heated to 500 °C. Anisole, also called methoxybenzene (C<sub>6</sub>H<sub>5</sub>O-CH<sub>3</sub>), was selected as a model compound because it represents a sample of the oxygenated aromatics found in biofuel intermediates. Moreover, its thermal stability and reported reaction pathways to desirable compounds such as phenolics and hydrocarbons simplify the process for evaluation catalytic activity.<sup>8-10</sup> Using a NE-1000 syringe pump from New Era, anisole entered the reactor system, vaporized, and mixed with the feed gas mixture, which bypassed the reactor for about 1 hr while the anisole feed steadied before being redirected to the catalyst for reaction tests. The experimental conditions are summarized in Table 1.

Table 1: Experimental Conditions for the HDO of Anisole over ZSM-5 Catalysts

Condition	Measurement
Model compound flowrate (cc/min)	0.1
H <sub>2</sub> gas flowrate (cc/min)	150
He gas flowrate (cc/min)	40
Ar gas flowrate (cc/min)	10
Catalyst mass (mg)	100
Reaction runtime (min)	60
Temperature (°C)	500

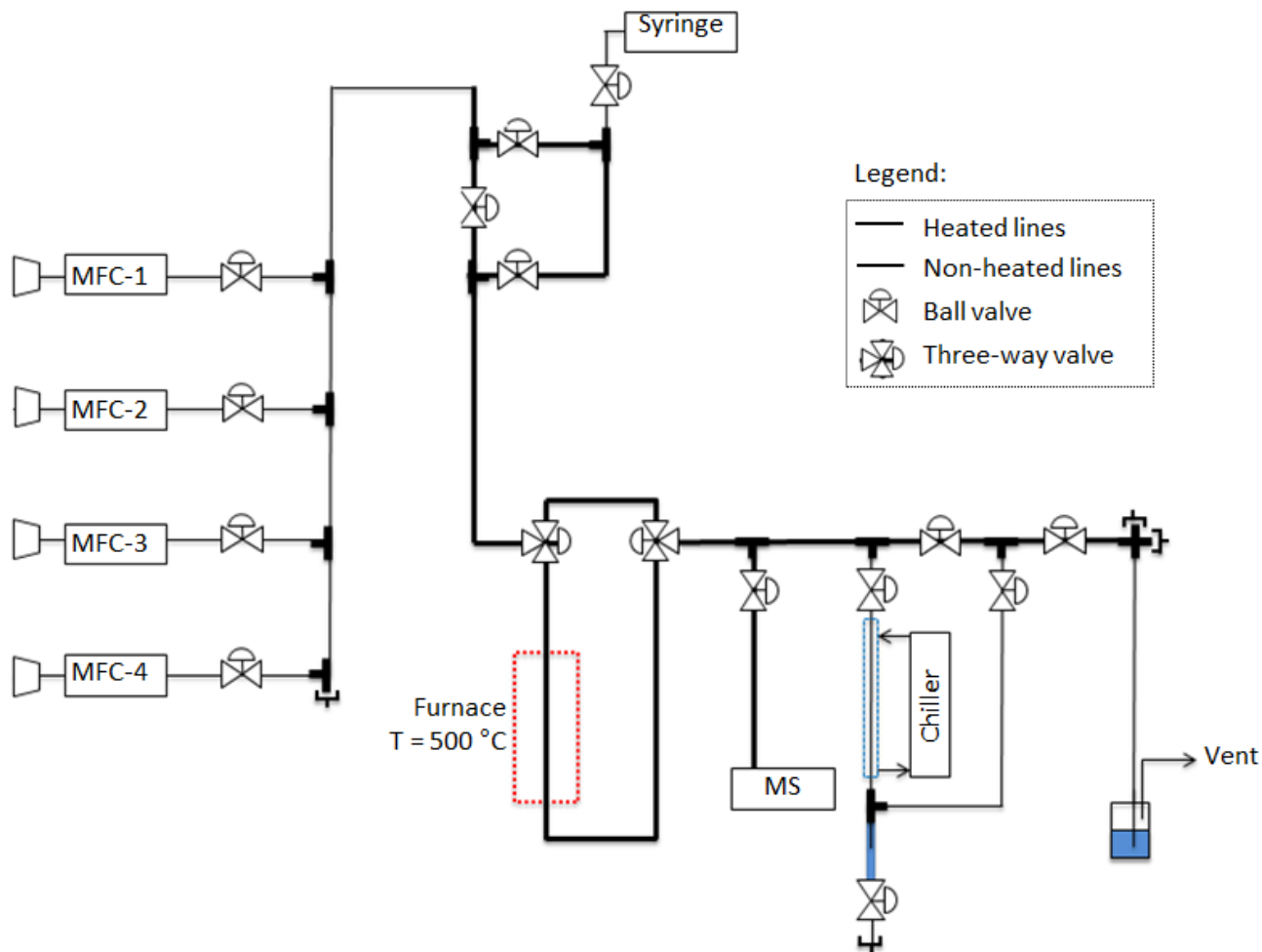


FIG. 2. Schematic of HDO reactor set-up. Gases leave the mass flow controllers (MFCs) and carry vaporized anisole from the syringe pump to the heated reactor before continuing to the MS for identification or the chilled tube for post-reaction liquid sample collection.

A Cirrus LM92 Mass Spectrometer from MKS Instruments identified the reaction products. The remaining post-reaction mixture was sent to a chilled tube kept at 5 °C, where the condensed liquid products were collected for analysis. To prevent anisole and reaction products from condensing prematurely, transfer lines were maintained at 120 °C using heat tapes. Figure 2 depicts a schematic of the reactor system above.

Analysis of each converted anisole liquid sample was conducted using a 7890A Model Gas Chromatograph (GC) / 5975C Model Mass Spectrometer (MS) from Agilent Technologies. Samples were diluted 1:99 in acetone, with pure anisole diluted in acetone serving as the control.

### III. RESULTS AND DISCUSSION

#### A. Catalyst Characterization

##### 1. Ammonia Temperature-Programmed Desorption

NH<sub>3</sub>-TPD was conducted to evaluate catalyst acidity before and after VPU. Each sample generated two TPD profiles from TCD signals: one before (TPD 1) and one after (TPD 2) regenerating in O<sub>2</sub>. These plots were then integrated to calculate the desorbed  $\mu\text{mol NH}_3/\text{g}$  catalyst, which reveals information about the number of acid sites. The TPD profiles for ZSM-5 are depicted in Figures 3 and 4 as an example. NH<sub>3</sub> desorption from the weak and strong acid sites explain the peaks at about 280 °C and 460 °C, respectively. H.J. Park et al.<sup>5</sup> reported similar peaks for ZSM-5. Table 2 shows the desorbed NH<sub>3</sub> values for each fresh and post-VPU (spent) sample.

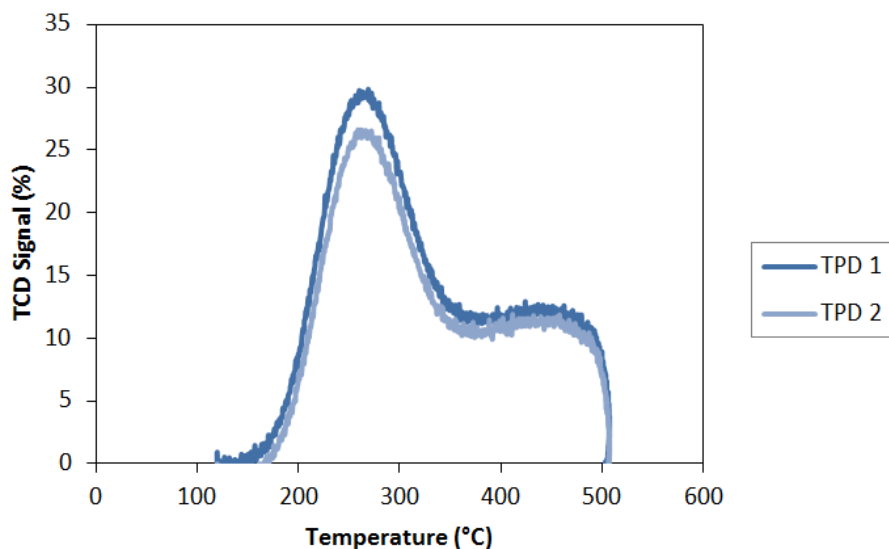


FIG. 3. NH<sub>3</sub>-TPD profiles of fresh ZSM-5

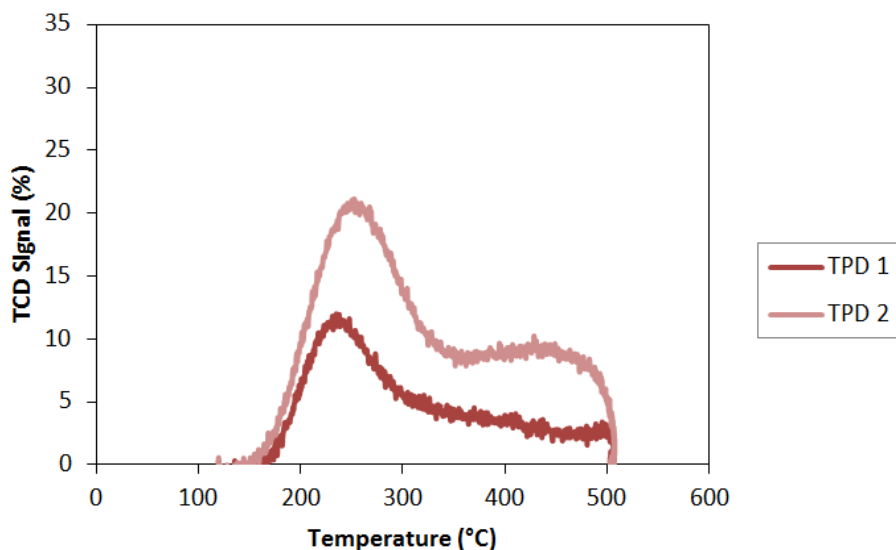


FIG. 4. NH<sub>3</sub>-TPD profiles of spent ZSM-5

Table 2: Desorbed NH<sub>3</sub> from ZSM-5 Catalysts

Catalyst	TPD 1 ( $\mu\text{mol NH}_3/\text{g catalyst}$ )		TPD 2 ( $\mu\text{mol NH}_3/\text{g catalyst}$ )	
	Fresh	Spent	Fresh	Spent
ZSM-5	802.2	332.3	782.0	606.1
Ni/ZSM-5	955.6	723.6	1168.5	929.8
Pt/ZSM-5	893.8	741.3	875.0	707.5
Cu/ZSM-5	853.8	788.1	1164.2	1209.7
Co/ZSM-5	1000.5	848.0	882.1	913.9
Ga/ZSM-5	928.5	537.5	975.8	754.8

Unmodified ZSM-5 had the least amount of desorbed NH<sub>3</sub> in all instances, indicating that it contains less acid sites than metal-modified ZSM-5 catalysts. For fresh samples, this may be attributed to Lewis acid sites that are added to the catalyst as a result of adding metal cations. For spent samples, this result suggests that adding metals to ZSM-5 reduces acid site blockage due to coke formation. Figure 5 illustrates the difference in NH<sub>3</sub> desorption between fresh and spent samples. All spent samples exhibited less NH<sub>3</sub> desorption than did fresh samples, signifying that coke formed on all catalysts. However, ZSM-5 retained only 41% of its acidity after VPU – the least amount of all catalysts tested – further validating the notion that metal-modified catalysts have improved resistance to coke formation. The percent acidity retained for each catalyst is listed in Table 3.

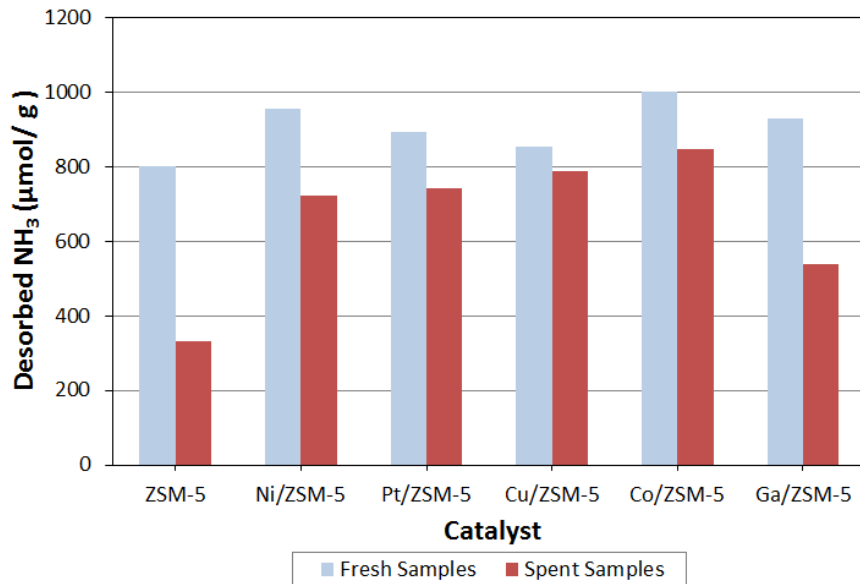


FIG. 5. NH<sub>3</sub> desorbed from fresh and spent samples



Table 3: Percent Acidity Retained in Spent ZSM-5 Catalysts

Catalyst	Acidity retained (%)
ZSM-5	41
Ni/ZSM-5	76
Pt/ZSM-5	83
Cu/ZSM-5	92
Co/ZSM-5	85
Ga/ZSM-5	58

## 2. X-ray Diffraction

The average crystalline size and phase state of metals added to ZSM-5 were determined through XRD analysis. Figures 6 and 7 show the diffraction patterns for fresh and spent samples, respectively, of each catalyst. Notably, Co/ZSM-5 and Ga/ZSM-5 have no observable diffraction peaks, which can be attributed to interference with ZSM-5. Another possible explanation is that Co and Ga dispersed well during metal impregnation, and therefore cannot be detected using XRD.

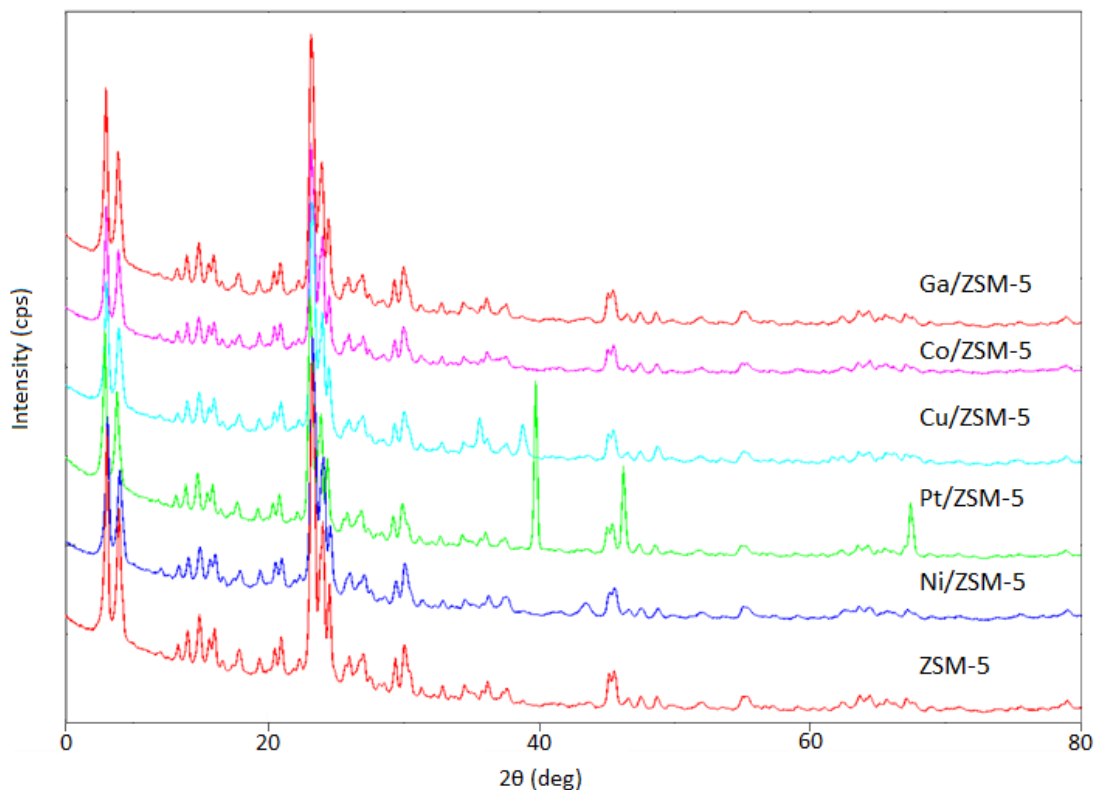


FIG. 6. XRD patterns of fresh samples ( $\lambda = 1.54 \text{ \AA}$ )

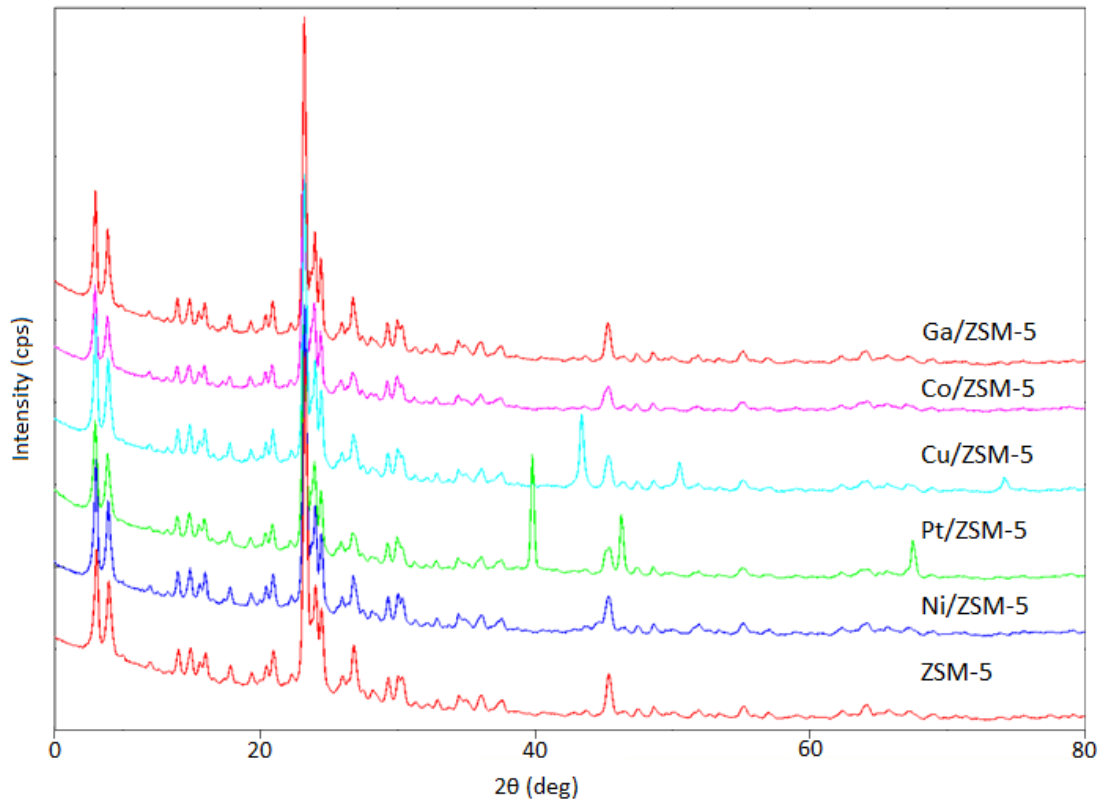


FIG. 7. XRD patterns of spent samples ( $\lambda= 1.54 \text{ \AA}$ )

Of the fresh samples, Ni/ZSM-5 has an observable peak at  $44^\circ$ ; Pt/ZSM-5 has peaks at  $39^\circ$ ,  $46^\circ$ , and  $67^\circ$ ; Cu/ZSM-5 has a peak at  $39^\circ$ . Because all catalysts were calcined during synthesis, all added metals were found to be in the oxide phase, except Pt, which was metallic. For spent samples, the peaks at  $43^\circ$  (Ni/ZSM-5) and  $42^\circ$  (Cu/ZSM-5) correspond to metallic phases of the added metals. Pt remained in the metallic phase, and therefore maintained the same peak locations as fresh Pt/ZSM-5.<sup>11-16</sup> The low-angle diffraction peaks ( $2\theta < 10^\circ$ ) present for all catalysts indicates that metal impregnation does not affect the orderly crystalline structure of ZSM-5. This agrees with a previous report on the physicochemical effects of metal impregnation.<sup>9</sup>

### 3. Nitrogen-Chemisorption

Catalyst porosity was evaluated via  $N_2$ -sorption. Total surface area was calculated using BET analysis, while BJH analysis was used to quantify pore surface area and pore volume. The contribution of micropores was distinguished using the t-plot method.

Figure 8 illustrates the effect of VPU on micropore surface area by contrasting fresh and spent samples. ZSM-5 demonstrated the greatest loss in micropore surface area (82%), whereas metal-modified catalysts retained more micropore surface area; notably, Pt/ZSM-5 lost only 24% of its micropore surface area. Likewise, when comparing pore volume for fresh and spent samples, as in Figure 9, it is apparent that ZSM-5 had the largest initial micropore volume and also lost the highest percentage of that volume post-VPU (81%). Again, metal-modified ZSM-5 catalysts showed less micropore volume loss, with Pt/ZSM-5 losing only 25%. Table 5 confirms

this trend, which can be attributed to coke filling the pores during VPU. Earlier studies have found that larger pores promote more rapid coke formation, since coke precursors have more room to form.<sup>4-6</sup> Indeed, Co/ZSM-5, which had the least initial micropore volume, also retained 72% of its volume post-VPU. Accordingly, the reduced micropore surface area and volume of metal-modified catalysts are favorable characteristics for resisting coke formation.

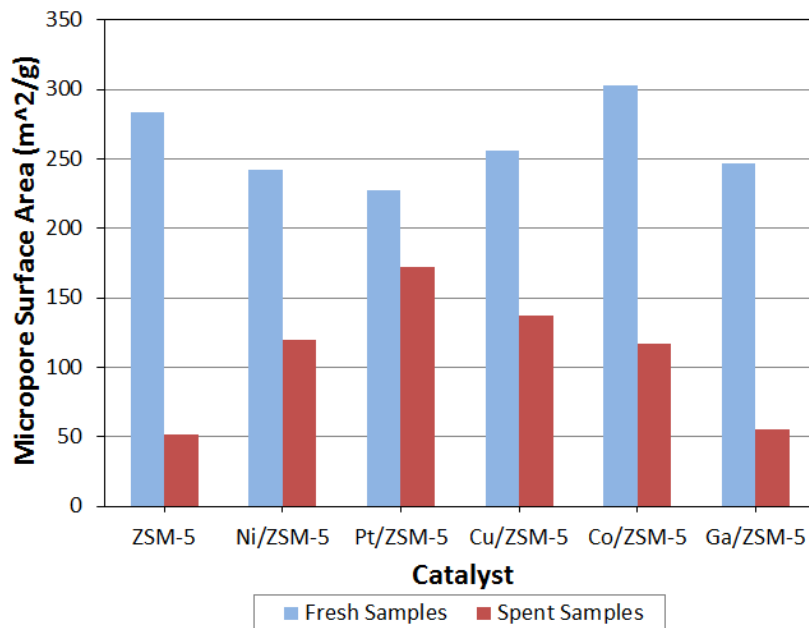


FIG. 8. Micropore surface area for fresh and spent samples

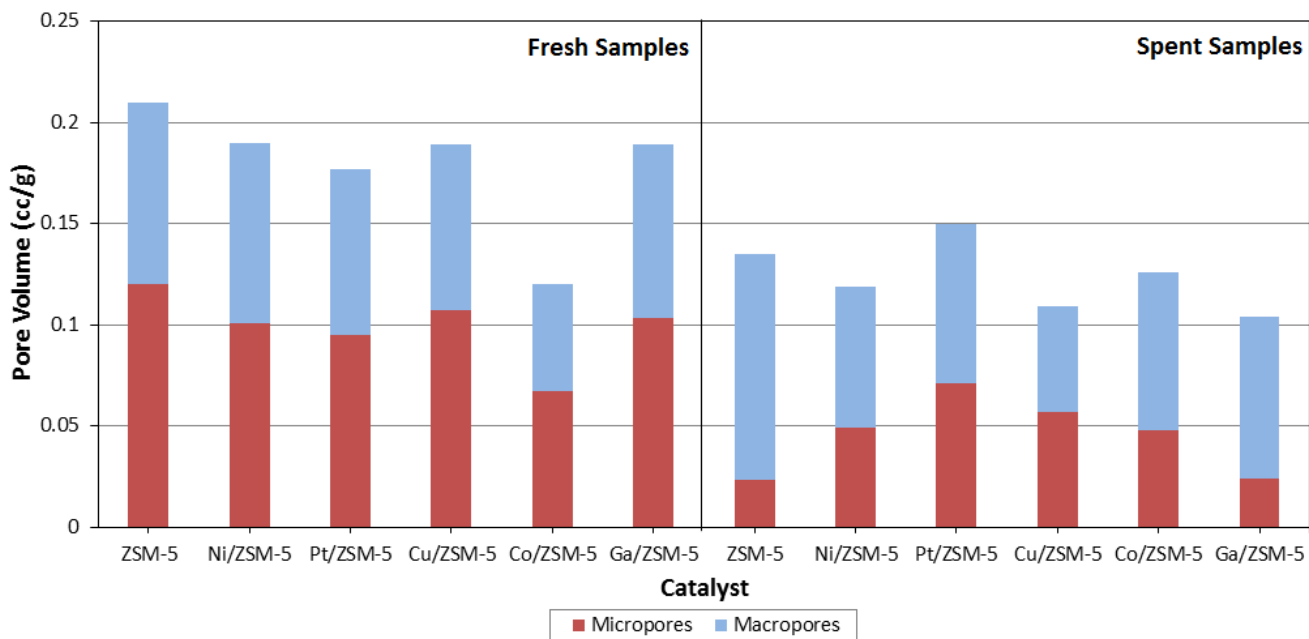


FIG. 9. Contribution of micropores and macropores to total pore volume of fresh and spent samples

Table 5: Effect of VPU on Micropore Surface Area and Volume in ZSM-5 Catalysts

Catalyst	Micropore Surface Area (m <sup>2</sup> /g)	Surface Area Lost (%)	Micropore Volume (cc/g)	Volume Lost (%)
ZSM-5	283.65	82	0.12	81
Ni/ZSM-5	242.34	50	0.101	51
Pt/ZSM-5	227.10	24	0.095	25
Cu/ZSM-5	256.21	46	0.107	47
Co/ZSM-5	302.79	61	0.067	28
Ga/ZSM-5	246.61	78	0.103	77

#### 4. Thermogravimetric Analysis

TGA was performed to quantify coke formation on spent catalysts by percent weight, displayed in Figure 10. ZSM-5 had the greatest amount of coke with 10 wt%; Pt/ZSM-5 had the least with 2.5 wt%. These results explicitly verify that metal-modified catalysts experience less coke formation, which is consistent with the findings from other characterization methods discussed in this study.

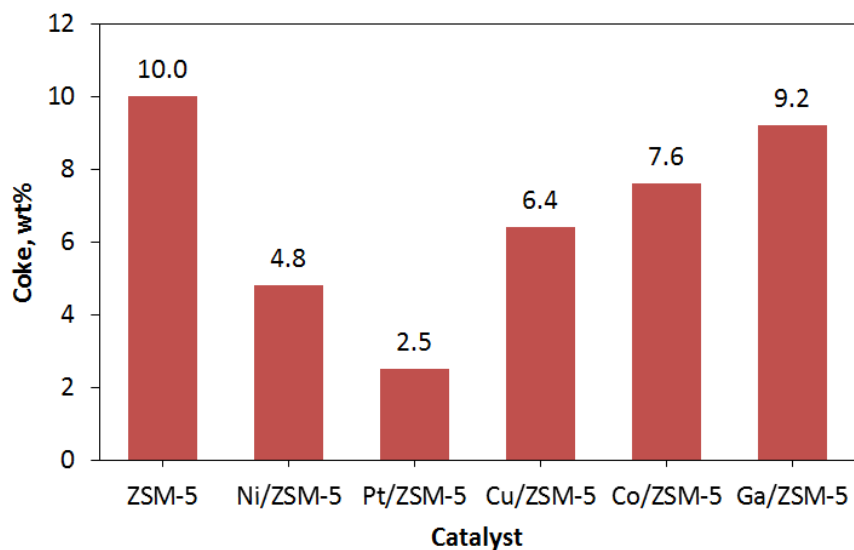


FIG. 10. Coke formation by weight percent on ZSM-5 catalysts

#### B. Catalytic Upgrading via VPU with pine

VPU was conducted with a 1:1 biomass-to-catalyst ratio to evaluate deoxygenation activity and catalyst stability. Pyrolysis vapors were directed to an MBMS, and the resulting chromatographs were normalized by the argon signal ( $m/z = 40$ ) for analysis.

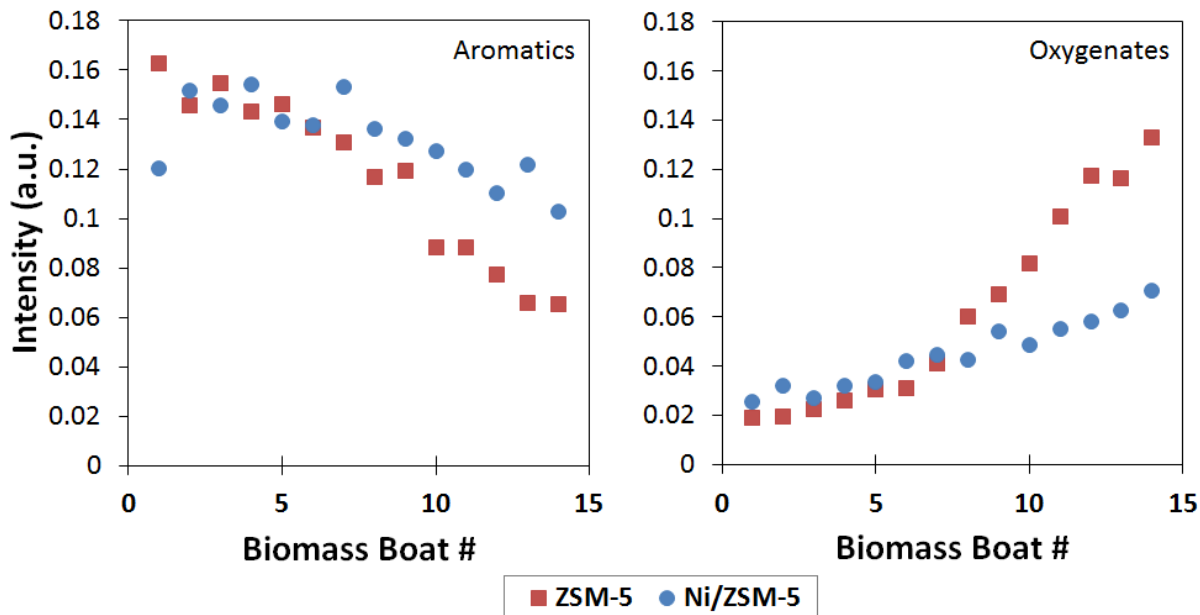


FIG. 11. Aromatic (benzene) production versus oxygenate (furan) production during VPU of pine over ZSM-5 and Ni/ZSM-5 catalysts. Intensity was normalized to the MBMS argon signal ( $m/z=40$ ).

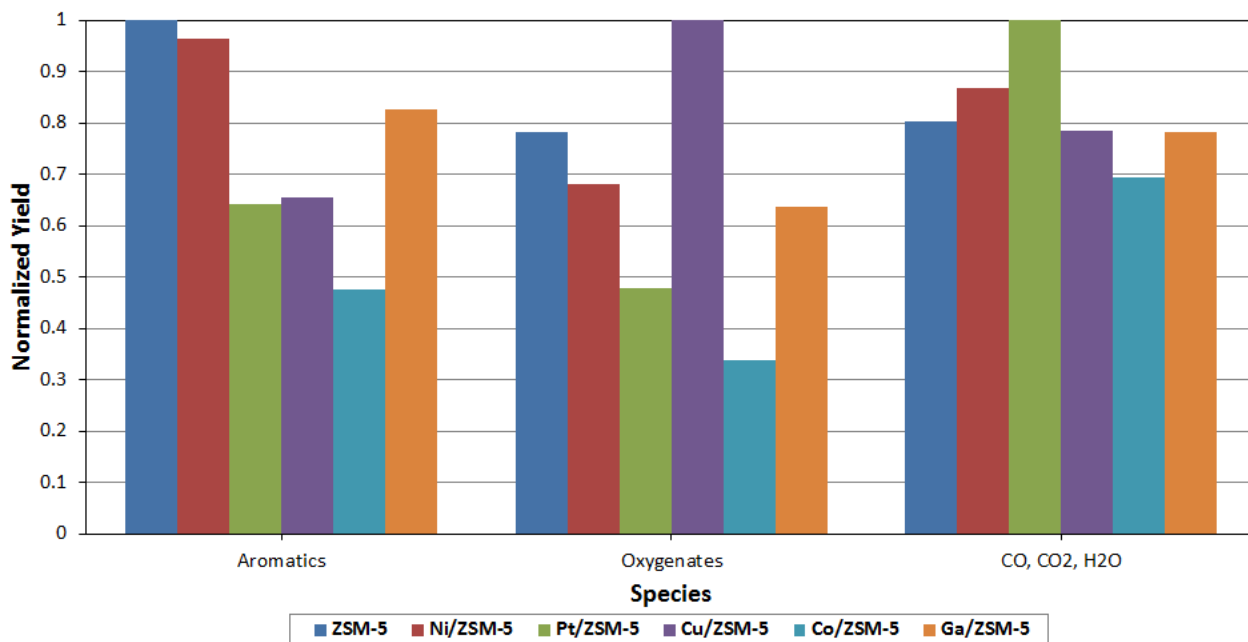


FIG. 12. Species yields normalized to maximum yield during VPU of pine

Figure 11 shows the intensity of benzene ( $m/z=78$ ) and furan ( $m/z=68$ ) production during VPU with ZSM-5 and Ni/ZSM-5. It is apparent that ZSM-5 initially yielded more benzene than did Ni/ZSM-5, which is supported by Figure 12, with ZSM-5 having the greatest normalized aromatic yield. However, ZSM-5 deactivated more rapidly than Ni/ZSM-5, as shown by the former's largely decreasing aromatic yield with each biomass boat. The rapidly increasing

furan, or oxygenate, yield of ZSM-5 (Figure 11) provides further evidence of deactivation. Although Ni/ZSM-5 had a lesser initial aromatic yield, its activity was more stable. Thus, over the entirety of the reaction, Ni/ZSM-5 yielded more aromatics than did ZSM-5. A previous study also found that catalysts with high aromatic product selectivity deposit larger amounts of carbon, creating coke.<sup>4</sup> This implies that high aromatic product selectivity is compromised for superior stability and sustained deoxygenation activity for metal-modified catalysts.

### C. Catalytic Upgrading via HDO with anisole

HDO reaction tests with anisole were conducted in a fixed-bed, vertical reactor to further investigate catalytic activity. Anisole conversion was calculated using the equation:

$$X = 1 - \frac{M_{108f}}{M_{108r}} \quad [\text{Eqn. 2}]$$

where  $M_{108f}$  is the average intensity of  $m/z=108$  (the molecular weight of anisole) during steady feed (bypassing the reactor) and  $M_{108r}$  is the average intensity of  $m/z=108$  during the HDO reaction. These intensity values were obtained from in-line MS signals.

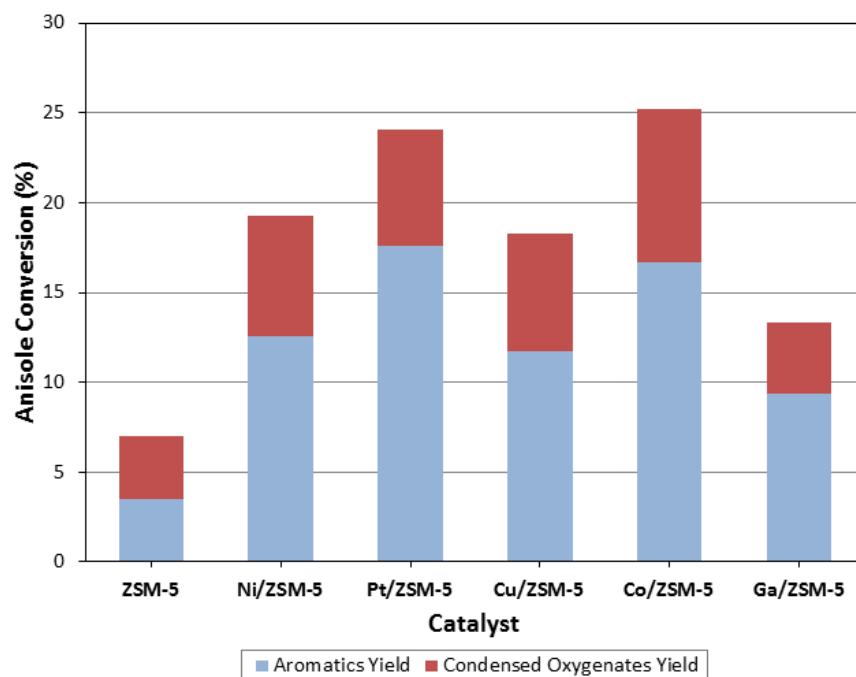


FIG. 13. Anisole conversion with aromatic and oxygenate product yields

The percent conversion of anisole, as well as the respective aromatic and oxygenate yields obtained from GC/MS analysis, are shown graphically in Figure 13, with exact values listed in Table 6. ZSM-5 Anisole conversion nearly doubled with the addition of metals to ZSM-5, with Co/ZSM-5 converting the most (25%). Considering that Co/ZSM-5 also had the most desorbed  $\text{NH}_3$  per gram during  $\text{NH}_3$ -TPD tests, this result agrees with an earlier study that found a proportional relationship between deoxygenation activity and the acidic properties of catalysts.<sup>5</sup>

All metal-modified catalysts also had superior hydrocarbon product selectivity compared to that of ZSM-5.

Table 6: Anisole Conversion and Hydrocarbon Product Selectivity during HDO with ZSM-5 Catalysts

Catalyst	Anisole Conversion (%)	Hydrocarbon Selectivity (%)
ZSM-5	7.0	50.0
Ni/ZSM-5	19.3	65.3
Pt/ZSM-5	24.1	73.0
Cu/ZSM-5	18.3	63.9
Co/ZSM-5	25.2	66.3
Ga/ZSM-5	13.3	70.7

Due to the volatility of aromatics, very little was collected in condensed liquid samples for GC/MS analysis. Therefore, aromatic product selectivity could not be directly observed. Instead, aromatic yield was calculated by taking the difference in average conversion for anisole ( $m/z = 108$ ) and benzene ( $m/z=78$ ) for each catalyst. Benzene was assumed to convert into the phenolics and other oxygenates identified through GC/MS analysis. The primary oxygenate species are represented in Figure 14 with their respective product selectivity.

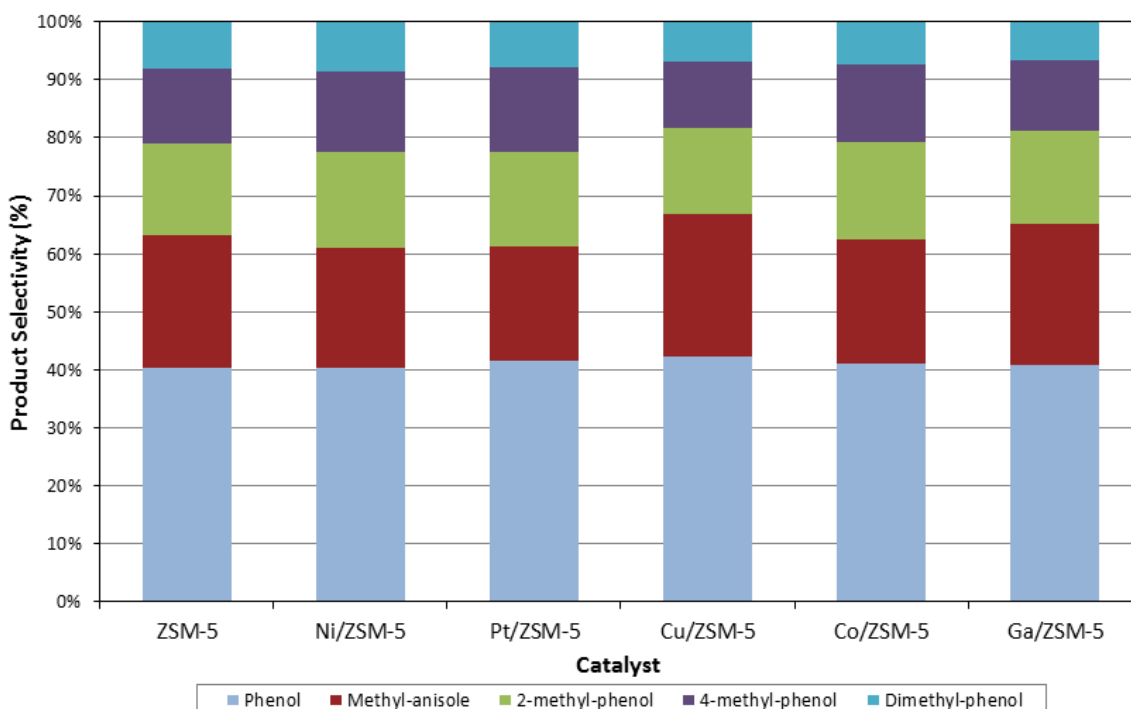


FIG. 14. Oxygenate product selectivity in ZSM-5 catalysts during HDO of anisole

Strikingly, the oxygenate product selectivity was nearly identical for all catalysts, in contrast to an earlier study.<sup>9</sup> This may be accredited to limitations of the reactor system or

analysis technique used. It could also suggest that adding metals to ZSM-5 does not affect the model compound reaction pathways.

#### IV. CONCLUSIONS AND FUTURE WORK

In summary, adding metals to ZSM-5 had favorable effects on acidity, porosity, and crystalline structure. These physicochemical properties were responsible for reduced coke formation, improved deoxygenation activity and advanced stability during catalytic upgrading of biofuel intermediates. These findings are important for developing competitive biofuels. Of the five metal-modified catalysts tested, Pt/ZSM-5 consistently outperformed the rest in terms of catalytic activity and coke resistance. However, it is not an economically ideal choice of catalyst due to the high cost of Pt. Ni/ZSM-5 and Co/ZSM-5 show comparable performances, and cost less to manufacture. Future studies may wish to optimize molar ratios during catalyst synthesis, or examine the influence of different reaction conditions on catalytic activity.

#### V. ACKNOWLEDGEMENTS

I would like to thank my research advisor, Matthew Yung, for his invaluable guidance and support. The following people were also instrumental to completing this work: Anne Sterace, Kellene McKinney, Steve Deutch, Matthew Sturgeon, and Susan Habas. This work was supported in part by the U.S. Department of Energy, Office of Science, Office of Workforce Development for Teachers and Scientists (WDTS) under the Science Undergraduate Laboratory Internship (SULI) program.

#### VI. REFERENCES

- <sup>1</sup> A.V. Bridgwater, "The production of biofuels and renewable chemicals by fast pyrolysis of biomass," *Int. J. Glob. Energy Issues*, **27**, 160-203 (2007).
- <sup>2</sup> M. Yung, (Private Communication)
- <sup>3</sup> S. Wan et al., "Decoupling HZSM-5 Catalyst Activity from Deactivation during Upgrading of Pyrolysis Oil Vapors," *ChemSusChem*, **8**, 552-559 (2015).
- <sup>4</sup> M. Guisnet and P. Magnoux, "Coking and Deactivation of Zeolites: Influence of the Pore Structure," *Appl. Catal.*, **54**, 1-27 (1989).
- <sup>5</sup> H.J. Park et al., "Highly valuable chemicals production from catalytic upgrading of radiate pine sawdust-derived pyrolytic vapors over mesoporous MFI zeolites," *Appl. Catal. B: Environ.*, **95**, 365-373 (2010).
- <sup>6</sup> M. Inaba et al., "Ethanol conversion to aromatic hydrocarbons over several zeolite catalysts," *React. Kinet. Catal. Lett.*, **88**, 135-142 (2006).
- <sup>7</sup> Micromeritics Instrument Corporation, "Temperature-Programmed Desorption (TPD) For Characterizing The Acid Sites On Oxide Surfaces," 11 Sep 2013,



<http://azonano.com/article.aspx?ArticleID=1475> (15 Feb 2015)

- <sup>8</sup> S.J. Hurff and M.T. Klein, "Reaction Pathway Analysis of Thermal and Catalytic Lignin Fragmentation by Use of Model Compounds," *Ind. Eng. Chem. Fundam.*, **22**, 426-430 (1983).
- <sup>9</sup> T.M. Sankaranarayanan et al., "Hydrodeoxygenation of anisole as bio-oil model compound over supported Ni and Co catalysts: Effect of metal and support properties," *Catal. Today*, **243**, 163-172 (2015).
- <sup>10</sup> J.E. Peters, J.R. Carpenter, and D.C. Dayton, "Anisole and Guaiacol Hydrodeoxygenation Reaction Pathways over Selected Catalysts," *Energy and Fuels*, **29**, 909-916 (2015).
- <sup>11</sup> G.L. Woolery et al., "On the nature of framework Bronsted and Lewis acid sites in ZSM-5," *Zeolites*, **19**, 288-296 (1997).
- <sup>12</sup> H. Qiao et al., "Preparation and Characterization of NiO Nanoparticles by Anodic Arc Plasma Method," *J. Nanomater.*, **2009**, 1-5 (2009).
- <sup>13</sup> T. Hyde, "Crystallite Size Analysis of Supported Platinum Catalysts by XRD," *Platinum Metals Rev.*, **52**, 129-130 (2008).
- <sup>14</sup> N. Tamaekong, C. Liewhiran, and S. Phanichphant, "Synthesis of Thermally Spherical CuO Nanoparticles," *J. Nanomater.*, **2014**, 1-5 (2014).
- <sup>15</sup> M. Rashad et al., "CuO and Co<sub>3</sub>O<sub>4</sub> Nanoparticles: Synthesis, Characterizations, and Raman Spectroscopy," *J. Nanomater.*, **2013**, 1-6 (2013).
- <sup>16</sup> C. Jin et al., "Annealing behavior of TiO<sub>2</sub>-sheathed Ga<sub>2</sub>O<sub>3</sub> nanowires," *J. Mater. Sci.: Mater. Electron*, **21**, 1154-1158 (2010).